

HEQuant: Marrying Homomorphic Encryption and Quantization for Communication-Efficient Private Inference

Tianshi Xu¹, Meng Li^{1,2}, Runsheng Wang¹

¹ School of Integrated Circuits, Peking University

² Institute for Artificial Intelligence, Peking University

meng.li@pku.edu.cn

Abstract

Secure two-party computation with homomorphic encryption (HE) protects data privacy with a formal security guarantee but suffers from high communication overhead. While previous works, e.g., Cheetah, Iron, etc, have proposed efficient HE-based protocols for different neural network (NN) operations, they still assume high precision, e.g., fixed point 37 bit, for the NN operations and ignore NNs' native robustness against quantization error. In this paper, we propose HEQuant, which features low-precision-quantization-aware optimization for the HE-based protocols. We observe the benefit of a naive combination of quantization and HE quickly saturates as bit precision goes down. Hence, to further improve communication efficiency, we propose a series of optimizations, including an intra-coefficient packing algorithm and a quantization-aware tiling algorithm, to simultaneously reduce the number and precision of the transferred data. Compared with prior-art HE-based protocols, e.g., CryptFlow2, Cheetah, Iron, etc, HEQuant achieves $3.5 \sim 23.4\times$ communication reduction and $3.0 \sim 9.3\times$ latency reduction. Meanwhile, when compared with prior-art network optimization frameworks, e.g., SENet, SNL, etc, HEQuant also achieves $3.1 \sim 3.6\times$ communication reduction.

1. Introduction

The last decade has witnessed the rapid evolution of deep learning (DL) as well as its increasing adoption in sensitive and private applications, including face authentication [1], medical diagnosis [22], personal assistant [3], etc. Privacy emerges as a major concern and leads to a growing demand for privacy-preserving DL [7, 9, 15, 29].

Secure two-party computation (2PC) based on homomorphic encryption (HE) has recently been proposed and attracted a lot of attention [8, 18, 24]. It helps to solve the dilemma between the DL model owner and the data

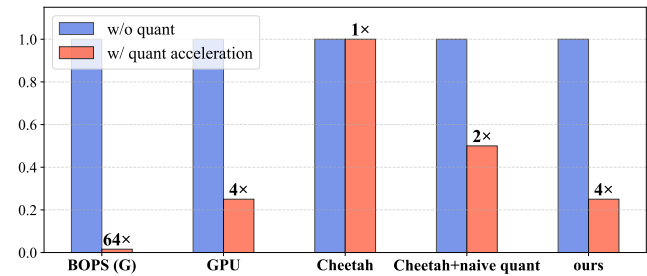


Figure 1. The acceleration achieved through network quantization (from 32-bit to 4-bit) on Bit Operations (BOPS), GPU, prior-art 2PC frameworks Cheetah and Cheetah with naive quant as well as our proposed framework.

owner: while the two parties want to jointly apply the model to the data, they do not want to give out the model or data directly. 2PC enables the computation and permits cryptographically-strong privacy protection [14, 16, 21, 29].

However, the privacy protection of the 2PC-based inference is achieved at the cost of high communication complexity since numerous high-precision ciphertexts (e.g., 109-bit ciphertext for Cheetah [18]) are transferred between the two parties. Previous works, e.g., Cheetah [18], Iron [16], Falcon [50], etc, have proposed efficient HE-based protocols for representative deep neural network (DNN) operations like convolutions, matrix multiplications, etc. However, they all assume high-precision plaintext operations (e.g., 37-bit plaintext for Cheetah [18]) are required and ignore the native robustness of deep neural networks (DNNs) towards quantization error [13]. As shown in Figure 1, prior works have shown that 4-bit quantization can achieve plausible accuracy with significant compute reduction [2, 10, 36, 51, 52], existing protocols like Cheetah cannot leverage such property for communication reduction.

While a naive combination of quantization and HE can help reduce the communication as shown in Figure 1, we find further efficiency improvement is challenging: on one hand, to ensure correct decryption, the plaintext modulus

Table 1. Notations used in the paper.

Notations	Meanings
$\lceil \cdot \rceil, \lfloor \cdot \rfloor, \text{round}(\cdot)$	Ceiling, flooring, and rounding operations
$\text{Enc}(\cdot), \text{Dec}(\cdot)$	Homomorphic encryption and decryption
$\boxplus, \boxminus, \boxtimes$	Homomorphic addition, subtraction and multiplication
P, Q	Plaintext modulus, and ciphertext modulus
N, p, q	Polynomial degree, bit width of plaintext ($p = \lceil \log_2 P \rceil$) and ciphertext ($q = \lceil \log_2 Q \rceil$)
b_x, b_w, b_{acc}	Bit width of activation, weight, and accumulation
H, W, C	Height, width, and channels of Conv2D input tensor
R, K	Kernel size and the number of kernels of Conv2D filters

cannot be reduced arbitrarily, leading to saturated efficiency gain for low-precision quantized networks, e.g., 4-bit or below; on the other hand, the input and output communication for a convolution layer is highly imbalanced while how to further reduce the output communication remains unclear.

In this paper, we propose a HE-based 2PC framework that is optimized for low-precision quantized DNN inference, named HEQuant. HEQuant features two main techniques to fully leverage the DNN quantization. First, HEQuant proposes an intra-coefficient packing algorithm to pack multiple input elements into each coefficient and allows further communication reduction given the saturated plaintext modulus. Moreover, HEQuant further proposes a novel quantization-aware tiling strategy for linear operations that significantly reduces output communication. Our main contributions can be summarized as follows:

- We observe existing HE-based 2PC frameworks are not optimized for quantization and propose HEQuant, the first 2PC framework that marries quantization and HE for efficient private inference.
- We propose an intra-coefficient packing algorithm and a quantization-aware tiling algorithm to further improve the communication efficiency for low-precision DNNs.
- HEQuant outperforms state-of-the-art (SOTA) HE-based 2PC frameworks, including CryptTFflow2, Cheetah and Falcon with $3.5 \sim 23.4\times$ communication reduction and $3.0 \sim 9.3\times$ latency reduction on CIFAR-100, Tinyimagenet and ImageNet datasets. Compared with prior-art network optimization algorithms, including ReLU-optimized networks and network pruning methods, HEQuant achieves $3.5\times$ communication reduction and $4.3\times$ latency reduction on average with higher accuracy.

2. Preliminaries

2.1. Threat Model

We focus on private DNN inference involving two parties, i.e., a server and a client. The server holds the model with private weights, while the client holds private inputs [16, 18, 50]. The model architecture, including the number of layers as well as the types, dimensions, and bit widths for

Table 2. Comparison with previous works. The Comm. is measured by Conv. with dimension (H,W,C,K,R)=(14,14,256,256,3) and ReLU with input dimension (14,14,256).

Framework	Protocol Opt.	Network Opt.	Conv. Comm.	ReLU Comm.
[5, 6, 20, 30]	-	ReLU Reduction	-	0.6 ~ 1 MB
[35]	-	Network Pruning	9 MB	2 MB
SiRNN[46]	Quantized MatMul Bit Extension/Trunc	16 bit Weight/Act. 40+ bit Accum.	9079 MB	15 MB
Cheetah[18]	HE Coeff.Pack for Conv/MatMul Output Coeff. Optim. ReLU Opt.	37 bit Quant.	12 MB	3 MB
Iron[16]	Tile for MatMul Softmax/GeLU Opt.	37 bit Quant.	14 MB	3 MB
HEQuant (ours)	Intra-Coeff.Pack for Conv/MatMul Tile for Conv Output Coeff. Optim.	Low-Precision Quant. e.g. 4/3 bit	4 MB	0.2 MB

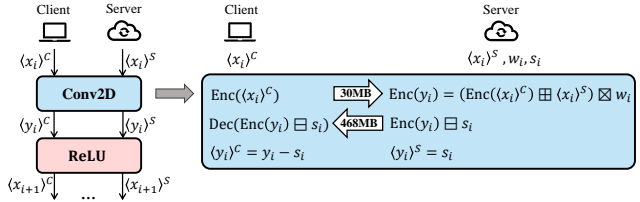


Figure 2. DNN private inference based on HE (linear layer).

each layer, is publicly known to both parties [38, 45]. At the end of the protocol execution, the client acquires the inference results without leaking any information to the server. Consistent with previous works [14, 19, 39, 46], we adopt an *honest-but-curious* security model where both parties adhere to the protocol’s specifications but also attempt to learn more than permitted. Hence, malicious attacks like adversarial attacks [33] are not the focus of the paper.

2.2. HE-based 2PC Inference

Related works There are often two categories of HE-based 2PC frameworks, including the end-to-end HE-based frameworks [11, 14, 23, 26, 31, 32, 41, 42] and the hybrid frameworks that combine both arithmetic secret sharing (ASS) and HE [12, 25, 34, 37, 38]. We focus on the second category as it supports different non-linear activations more accurately [16, 18, 21, 45, 50]. We compare HEQuant with existing works including 2PC frameworks[16, 18, 46] and network optimization works[5, 6, 20, 30, 35], as shown in Table 2. HEQuant leverages an intra-coefficient packing for convolution with tiling and output coefficient optimization. Furthermore, HEQuant utilizes low-precision network quantization and significantly reduces both linear and non-linear layers’ communication. In addition, we summarize the notations used in the paper in Table 1.

The flow of 2PC-based inference Figure 2 shows the flow of 2PC-based inference. With ASS, each intermediate activation tensor, e.g., x_i , is additively shared where the server holds $\langle x_i \rangle^S$ and the client holds $\langle x_i \rangle^C$ such that $x_i = \langle x_i \rangle^S + \langle x_i \rangle^C \pmod P$ [39]. For a linear layer, e.g. Conv2D, to compute the result of y_i without revealing both parties’ information, the client first encrypts its share as

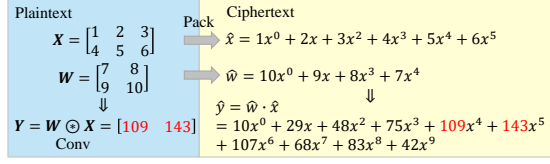


Figure 3. A convolution example of coefficient packing.

Table 3. Comm. complexity of HE-based 2PC frameworks.

Layer Type	Linear Layer (Conv.)		Non-linear Layer
	Input Ciphertext	Output Ciphertext	
Comm. Complexity	$\lceil \frac{HWC}{N} \rceil \times Nq$	$(\lceil \frac{HWC}{N} \rceil \times N + HWK)q$	$O(b_x)$

$\text{Enc}(\langle x_i \rangle^C)$ and sends it to the server. Since HE supports homomorphic addition and multiplication without the need for decryption, the server can compute $\text{Enc}(y_i)$ and blind y_i by subtracting a randomly sampled s_i . Finally, the server sends the result to the client for decryption. The server and client now obtain the secret shares of the Conv2D output y_i ¹. For a non-linear layer, e.g. ReLU, we omit the detailed protocols and refer interested readers to [18, 45, 46].

At a lower level, HE encrypts the plaintexts into ciphertext polynomials and computes over the polynomials, which can be regarded as 1-dimensional vectors. In contrast, DNN processes high-dimensional tensors. Therefore, packing becomes necessary to encode tensors into polynomials. Cheetah [18] identifies that polynomial multiplications natively perform convolution operations and introduces a polynomial coefficient packing method. In this approach, elements in tensors are encoded into coefficients, and the correct result can be extracted from the outcome of polynomial multiplication. A toy example is illustrated in Figure 3.

2.3. Communication Complexity of HE-based 2PC

The communication of a linear layer is mainly consumed by the input and output ciphertext transfer. The communication can be accurately estimated by the product of the number of ciphertext polynomials and the size of each polynomial. For each polynomial, the communication is the product of the polynomial degree and the bit width of each coefficient. Hence, the communication of the input ciphertexts can be estimated as $\#Poly \times Nq$. For the output ciphertext, because each activation is encrypted into a scalar b and a polynomial a , extra scalars need to be transferred. Hence, following Cheetah [18], the output communication can be estimated with $\#Poly \times Nq + nq$, where n is the number of output activations, $\#Poly \times Nq$ is the communication of a , and nq is the communication of b . For a non-linear layer like ReLU, the communication scales with the

¹Note it is possible to move the HE computation to the pre-processing stage [38], the required total communication remains almost the same.

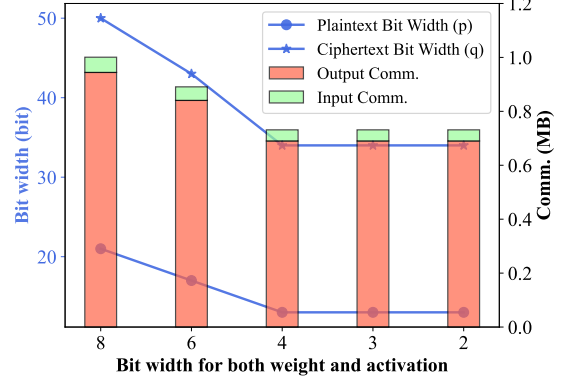


Figure 4. The input and output communication as well as the bit width of plaintext and ciphertext for different bit precision quantization.

bit width of activations b_a [46]. We summarize the communication complexity in Table 3.

Operator tiling for linear layer When the input tensor size gets larger than the polynomial degree, it needs to be tiled into a group of small tensors before encoding into polynomials. Operator tiling determines the strategy of splitting the input tensors and directly impacts the communication cost [16]. For a general convolution, previous works [16, 50] focus on minimizing the communication of input polynomials, i.e., they try to pack as many input activations as possible. Hence, following Cheetah, given N , the numbers of input polynomials and output polynomials are $\lceil \frac{HWC}{N} \rceil$ and $\lceil \frac{HWC}{N} \rceil$, respectively [18].

Selection of HE parameters p and q In HE, p represents the bit width of the plaintext field. To avoid overflow, the lower bound of p is the required accumulation bit width for a linear layer, i.e., b_{acc} . Given p , $q - p$ determines the noise budget of the HE-based computation, which is determined by the depth of multiplications. In addition, we introduce the background of network quantization in Appendix A.

3. Motivation

In this section, we discuss the key observations that motivate our quantized HE-based 2PC framework HEQuant. We will focus on the linear layers as they contribute to the majority of the communication [16, 18, 37].

Observation 1: both HE parameters p and q can be reduced for low-precision quantized DNN linear operators, leading to better communication efficiency. As introduced in Section 2.3, for a linear operator, p is determined by the accumulation bit precision while $q - p$ is determined by the required noise budget and is roughly fixed for a given operator. Low-precision quantization helps to directly reduce the required accumulation bit precision, and thus, improves the communication efficiency. The observation is also verified in Figure 4. Considering the robustness

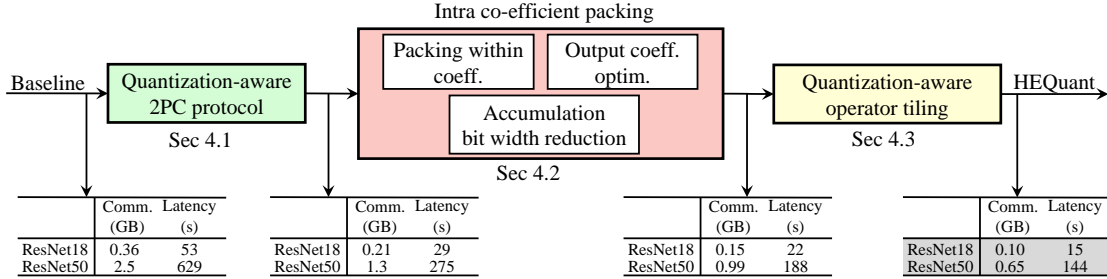


Figure 5. Overview of HEQuant and the communication/latency cost after each optimization step. The examples are ResNet18 on CIFAR-100 and ResNet50 on ImageNet. Coeff. represents coefficient.

of DNNs to quantization error [13, 28, 40], low-precision quantization becomes a promising technique to improve the efficiency of the HE-based 2PC framework.

Observation 2: while networks continue to be quantized for sub-4-bit precision, p and q cannot be further reduced, leading to saturated communication efficiency improvement. Previous research has demonstrated the feasibility of quantizing networks to sub-4 bits, such as 2-bit or even 1-bit, while maintaining comparable accuracy [36, 43, 44, 53]. However, as shown in Figure 4, we empirically find p cannot be reduced below 13 bits to ensure correct computation, leading to saturated communication reduction, especially for sub-4-bit quantization. Hence, how to further improve the communication efficiency for ultra-low precision quantized DNNs is also an important question to answer.

Observation 3: the input and output communication are not balanced. As shown in Figure 4, regardless of the bit precision, the communication of output ciphertexts is much larger compared to the input ciphertexts as more output ciphertexts need to be transferred. Table 3 also theoretically supports it. While past research has proposed to tile the input for matrix multiplications and depthwise convolutions to reduce the number of output polynomials [16, 50], a general tiling algorithm has not yet been proposed for convolutions especially when considering the impact of quantized DNNs. Moreover, as introduced in Section 2.3, another way to reduce output communication is to lower the coefficient bit widths. Hence, how to reduce the coefficient bit precision beyond q without impacting the output correctness is also an important direction to study.

4. HEQuant: Communication-Efficient 2PC Framework

In this section, we present HEQuant, an efficient 2PC framework based on quantization-aware HE protocols. The overview of HEQuant is shown in Figure 5. Based on Observation 1, given a quantized network, we first propose a quantization-aware 2PC protocol and optimize the communication by reducing the HE parameters p and q , achiev-

ing more than $2\times$ latency reduction (Section 4.1). Then, to further improve the efficiency, we propose intra-coefficient packing to allow packing multiple low-precision activations into a single coefficient to reduce the number of input and output ciphertexts. A series of bit width optimizations for both the plaintext and ciphertext, i.e., p and q , are also developed to enable dense packing. The proposed optimization further enables $1.4\times$ latency reduction (Section 4.2). In the last step, a quantization-aware tiling algorithm is proposed for general linear operations (Section 4.3). With 3-bit weight and 3-bit activation, HEQuant achieves almost $4\times$ latency reduction over prior-art Cheetah framework [18].

4.1. HE-based quantized private inference

Based on the observations discussed in Section 3, We propose the quantized HE-based 2PC frameworks in Figure 6. We take a residual block as an example. To avoid overflow, the HE-based convolution protocol requires the plaintext bit width $p \geq b_{acc}$. However, the convolution input is b_a -bit. Hence, bit extension protocols are needed to increase the bit width of activations from b_a -bit to b_{acc} -bit. After the convolution, we truncate output activations from b_{acc} -bit to b_a -bit to conduct low-precision ReLU to reduce communication since the communication of ReLU scales linearly with the activation bit width as shown in Table 3. The bit width extension, truncation, and residual protocols are all implemented following previous work SiRNN [46]. We refer interested readers to [46] and focus on describing the quantization-aware HE-based convolution protocol in the following sections.

4.2. Intra Co-efficient Packing

Packing within coefficient Following Observation 2 in Section 3, the communication reduction saturates for sub-4-bit quantized linear layers due to the lower bound of p and q . We observe although p and q cannot be further reduced, it is possible to pack multiple low-precision activations into a single coefficient. Consider the example in Figure 7. Two 4-bit values are packed into one 18-bit coefficient with the two values occupying 0 – 4 and 9 – 13 bits, respectively.

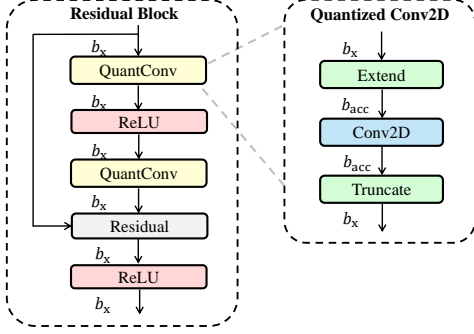


Figure 6. Quantized HE-based 2PC frameworks on a residual block. b_x means the bit width for activation.

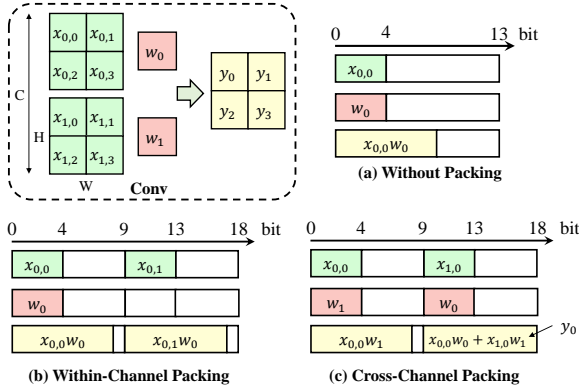


Figure 7. Examples of the proposed intra coefficient packing.

Such packing strategy enables us to correctly compute one multiplication with a 4-bit weight and one accumulation (which at most requires 9-bit accumulation) while reducing the number of coefficients by $2\times$. Based on the observation, for a convolution, we propose two strategies for intra-coefficient packing, namely Within-Channel Packing and Cross-Channel Packing.

Within-Channel Packing As shown in Figure 7 (b), Within-Channel Packing combines two activations within the same channel into one coefficient. Since these two activations need to multiply the same weight, the weight packing stays the same. After the homomorphic multiplication, each coefficient will also have two output activations, resulting in a $2\times$ reduction in the input and output polynomials as well as the number of output coefficients.

Cross-Channel Packing Figure 7 (c) shows the Cross-Channel Packing strategy. Two activations along the same channel are now packed into the same coefficient. Since the two activations need to multiply different weights and the products need to be added together, the weights packing needs to be modified accordingly. After the homomorphic multiplication, each coefficient only contains one output activation in higher bit locations. Hence, Cross-Channel Packing reduces the input and output polynomials by $2\times$ while

Table 4. Comparison of packing methods on communication and limitation as well as the measured communication for a Conv. with dimension $(H,W,C,K,R)=(14,14,32,32,1)$, $b_{acc} = 8$. “+” represents output coefficient optimization. The actual value for p and q can be different for Cheetah and our method.

Packing Method	Input Comm.	Output Comm.	Conv. Comm.	Limitation
Cheetah	$\lceil \frac{HWC}{N} \rceil \times Nq$	$(\lceil \frac{HWC}{N} \rceil \times N + HWK)q$	0.90 MB	-
Within-Channel	$\lceil \frac{HWC}{2N} \rceil \times Nq$	$(\lceil \frac{HWC}{2N} \rceil \times N + \frac{HWK}{2})q$	0.51 MB	kernel size=1
Cross-Channel	$\lceil \frac{HWC}{2N} \rceil \times Nq$	$(\lceil \frac{HWC}{2N} \rceil \times N + HWK)q$	0.52 MB	/
Within-Channel+	$\lceil \frac{HWC}{2N} \rceil \times Nq$	$\lceil \frac{HWC}{2N} \rceil \times N(p + \sigma) + \frac{HWKp}{2}$	0.33 MB	kernel size=1
Cross-Channel+	$\lceil \frac{HWC}{2N} \rceil \times Nq$	$\lceil \frac{HWC}{2N} \rceil \times N(\frac{q}{2} + \sigma) + HWKp$	0.23 MB	1-bit error

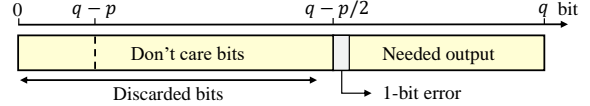


Figure 8. Output coefficient optim. by discarding low-end bits.

the number of output coefficients remains unchanged.

Comparison These two packing schemes have different advantages and disadvantages and are suitable for different situations. For one thing, Cross-Channel Packing can be applied to convolution with any kernel size while Within-Channel Packing can only be used for convolution with kernel size 1. For another, they also have different communication impacts as summarized in Table 4. As can be observed, Within-Channel Packing achieves smaller output communication due to fewer output activations. Additionally, we observe that in Cross-Channel Packing, only the higher bit locations of each output activation are useful. This indicates opportunities to further optimize the communication as will be discussed later.

Output coefficient optimization To further reduce the communication of output ciphertext, we further reduce the coefficient bit widths of output ciphertexts. Our bit width optimization is based on the following two observations. Firstly, recall from Section 3, a p -bit output m is encrypted into a scalar b and a polynomial a . During decryption, we compute $m = \lfloor (b + a^T s)P/Q \rfloor$ to reconstruct the output m , where Q and P are the ciphertext modulus and plaintext modulus, respectively. Hence, the low $q - p$ bits of each coefficient may not be fully needed. Secondly, as mentioned above, in our Cross-Channel Packing method, only the higher bit locations of each coefficient are useful while the other bits may not be fully required for decryption. We illustrate the observations in Figure 8.

Based on the observations, we propose to discard the lower bits before ciphertext transmission. We observe discarding these lower bits is equivalent to truncating coefficients and may introduce a single-bit error after truncation. The error probability depends on the number of discarded bits. Moreover, since each output activation is encrypted into a scalar b and a polynomial a , how to discard b or a

will lead to different error rate and communication. We empirically decide to skip the low $\lfloor \log_2(Q/P) \rfloor - 1$ of b and the low $\lfloor \log_2(Q/P) \rfloor + \frac{p}{2} - 1 - \sigma$ of a during output ciphertext transmission, where σ is the standard deviation of $a^T s$. Additional details are available in Appendix B and in the experimental results, a comprehensive ablation study justifies this choice.

With the output coefficient optimization, the communication complexity of the two packing methods proposed above is shown in Table 4, denoted as ‘‘Within-Channel+’’ and ‘‘Cross-Channel+’’.

Accumulation bit width reduction As analyzed in Section 2.3, the plaintext bit width p is selected according to the accumulation bit width b_{acc} . Hence, how to reduce the accumulation bit width directly impacts the inference cost. We adopt three strategies to estimate the required b_{acc} .

Strategy 1 We directly set $b_{acc} = b_w + b_x + \log_2(e)$ to avoid any overflow, where e is the number of accumulations. This is extensively used in previous works [2, 36, 46, 51]. However, we find that accumulated values rarely reach the theoretical upper bound as the weights can be either positive or negative and most weights have small magnitude and do not reach 2^{b_w} . Hence, we propose Strategy 2 to reduce the accumulation bit width.

Strategy 2 Considering the weights are frozen during inference, for one output channel, we have $\sum_{i=1}^e |x_i w_i| \leq \sum_{i=1}^e |x_i| |w_i| \leq 2^{b_x} \sum_{i=1}^e |w_i| = 2^{b_x} \|\mathbf{w}\|_1$. So we just need $b_{acc} = b_x + \lceil \log_2(\|\mathbf{w}\|_1) \rceil$ to avoid overflow. A weakness is that it may leak $\lceil \log_2(\|\mathbf{w}\|_1) \rceil$. However, we find it’s still hard for the client to obtain weights.

Strategy 3 We further observe that most activations also cannot reach the upper bound of 2^{b_x} . Hence, we propose to leverage the training dataset to directly collect the accumulation bit width required for each layer. While this minimizes b_{acc} , it may introduce the overflow error if the testing dataset does not follow the same statistics as the training dataset. We compare the three strategies in Section 5.4 and empirically find Strategy 3 does not impact the model testing accuracy. We also show the layer-wise accumulation bit width comparison of three strategies in Appendix C.

4.3. Quantization-aware operator tiling

Based on Observation 3 in Section 3, the input and output ciphertext communication are highly imbalanced, which motivates previous works to tile the operator to minimize the communication. Specifically, Iron and Falcon design tiling strategies for matrix multiplication and depthwise convolution, respectively. However, we find there exist two main drawbacks in previous methods: **1)** lack of tiling strategy for general convolution; **2)** do not consider the layer-wise difference in p, q induced by the network quantization and output coefficient optimization.

To address these issues, we propose a novel quantization-

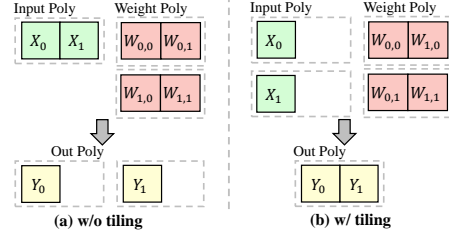


Figure 9. A toy example of operator tiling where each square means a channel and $W_{0,1}$ means the second channel of the first kernel of the filter.

aware tiling algorithm for general convolution. We first conduct a theoretical analysis of communication cost and formulate it as a nonlinear programming problem. Based on Section 2.3, when introducing tiling at the channel level, we use C_x, C_w to denote the number of input and weight channels in each polynomial, respectively. Then the communication cost is given by the equation:

$$\lceil \frac{C}{C_x} \rceil \times Nq + (\lceil \frac{K}{C_w} \rceil \times N + HWK)q \quad (1)$$

where $\lceil \frac{C}{C_x} \rceil$ and $\lceil \frac{K}{C_w} \rceil$ are the number of input and output polynomials, respectively. Furthermore, when output coefficient optimization is introduced, the communication cost of Equation 1 can be replaced by that in Table 4.

Now we formulate the tiling optimization problem as a nonlinear programming problem. Note that in Equation 1, only C_x, C_w needs to be determined, with all other parameters are known before execution. Moreover, we have two constraints: **1)** polynomial coefficient encoding should not exceed the degree N , and **2)** C_x must be a positive integer multiple of C_w to avoid doubling of the number of multiplications. Consequently, the tiling optimization problem can be formulated as follows:

$$\begin{aligned} \min \quad & \lceil \frac{C}{C_x} \rceil \times Nq + (\lceil \frac{K}{C_w} \rceil \times N + HWK)q \\ \text{s.t.} \quad & C_x HW \leq N \\ & C_x = kC_w \text{ where } k \in \mathbb{Z}^+ \end{aligned}$$

This is a solvable nonlinear programming problem with a relatively small solution space. With $C_x \leq \frac{N}{HW}$ and $C_x = kC_w$, the solution space is at most $\frac{N}{HW} \times \frac{N}{HW}$, enabling direct solution through a search algorithm with a complexity of $O((\frac{N}{HW})^2)$. An example is illustrated in Figure 9, after tiling, we reduce the size of output polynomials.

5. Experimental Results

5.1. Experimental Setup

HEQuant is built on top of the SEAL library [47], the EMP toolkit [49] and OpenCheetah [18] in C++. We also use

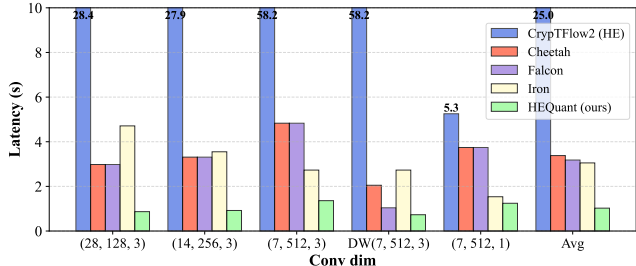


Figure 10. Latency comparison of convolutions of different dimensions (Conv dim represents the input feature height, channels, and kernel size). DW means depthwise convolution and Avg means the average.

the Ezpc library [4] to evaluate CryptFlow2 [45]. Consistent with [18, 39, 48], we simulate a LAN and WAN network setting via Linux Traffic Control, where the bandwidth is 384 MBps and 9 MBps, respectively. All the following experiments are performed on machines with 2.2 GHz Intel Xeon CPU. Following [16, 18], we set $N = 4096$. For network quantization, we use PyTorch framework for quantization-aware training, and for the inference accuracy evaluation. We follow [2]’s setting to train ResNet18 on CIFAR-100 and Tinyimagenet with different bit width, including W8A8, W4A4, W3A3, W2A3 (WxAy means x-bit weights and y-bit activation). We follow the setting of [51] to train ResNet50 on ImageNet with bit width W8A8, W4A4, W3A3 and W2A2. What’s more, we use strategy3 for HEQuant to determine the accumulation bit width. The more training details are shown in Appendix D.

5.2. Micro-Benchmark Evaluation

We compare the performance of HEQuant with CryptFlow2, Iron, Cheetah, and Falcon for single convolution and depthwise convolution with different dimensions. We determine the accumulation bit width based on W4A4 for HEQuant. As shown in Figure 10, HEQuant achieves on average $3.0\times$ latency reduction compared to SOTA Iron. Note that due to the use of SIMD-based HE in CryptFlow2, there is an extremely high latency [18]. In comparison, HEQuant achieves a notable latency reduction of $31\times$. We also provide the results of communication in Appendix F.

5.3. End-to-End Inference Evaluation

Benchmark with prior-art 2PC frameworks We first benchmark HEQuant with prior-art 2PC frameworks which focus on secure protocols’ improvement, including Cheetah, Falcon, CoPriv, etc [18, 45, 46, 50, 54]. We conduct the end-to-end private inference in our quantized networks with different bit widths. We draw the Pareto curve of accuracy and communication/latency (LAN) in Figure 11. We put results of latency under WAN in Appendix E.

Table 5. Communication (MB) comparison with different accumulation bit width reduction strategies.

Network and Dataset	Cheetah	HEQuant (Strategy1)	HEQuant (Strategy2)	HEQuant (Strategy3)
ResNet18 (Cifar100)	362	153 (2.4 \times ↓)	141 (2.6 \times ↓)	102 (3.6 \times ↓)
MobileNetV2 (Tinyimagenet)	608	132 (4.6 \times ↓)	123 (4.9 \times ↓)	114 (5.3 \times ↓)
ResNet50 (Imagenet)	2454	771 (3.2 \times ↓)	689 (3.7 \times ↓)	654 (3.8 \times ↓)
Average	1141	352 (3.24 \times ↓)	318 (3.59 \times ↓)	290 (3.94 \times ↓)

Result and analysis From Figure 11, we make the following observations: **1)** HEQuant achieves SOTA pareto front in all three benchmarks. More specifically, compared with Cheetah, HEQuant achieves $3.0\times$ communication and $3.9\times$ latency reduction in ImageNet. Compared with cheetah with the same quantization bit width, HEQuant achieves $2.0 \sim 2.3\times$ communication reduction and $1.4 \sim 1.9\times$ latency reduction in three benchmarks, respectively. Moreover, HEQuant achieves 2.3% higher accuracy with less latency in ImageNet. **2)** Compared with OT-based frameworks, SiRNN and CoPriv [54], HEQuant demonstrates strong superiority and outperform them with $52 \sim 83\times$ and $91 \sim 111\times$ communication reduction, respectively. This translates to a latency improvement of an order of magnitude under WAN, as shown in Appendix E. Since Falcon is specifically optimized for MobileNet with depthwise convolution, we compare HEQuant with Falcon on MobileNetV2 in Appendix G and demonstrate $2.5\times$ communication reduction.

Benchmark with prior-art network optimization algorithms Since HEQuant requires to quantize the network, we also benchmark HEQuant with other different network optimization algorithms, including ReLU-optimized networks (SENet, SNL, DeepReduce, etc) and SOTA network pruning methods (MetaPruning and uniform pruning) [6, 20, 30, 35]. We apply those algorithms to the 2PC framework Cheetah and draw the Pareto curve in Figure 12.

Result and analysis From the results in Figure 12, we observe: **1)** Compared with ReLU-optimized networks, HEQuant achieves over $3\times$ communication by both reducing the linear and non-linear layers’ communication; **2)** Compared with network pruning method MetaPruning, HEQuant achieves $3.6\times$ communication reduction and $4.2\times$ latency reduction as well as 1.1% higher accuracy in ImageNet.

5.4. Ablation Study

Accumulation bit width reduction strategies In Table 5, we show the communication of different accumulation bit width reduction strategies. We find that even with Strategy 1, HEQuant still achieves $3.2\times$ communication reduction compared with Cheetah. With Strategy 3, HEQuant achieves on average $3.9\times$ communication reduction over Cheetah.

Output coefficient optimization analysis To show the

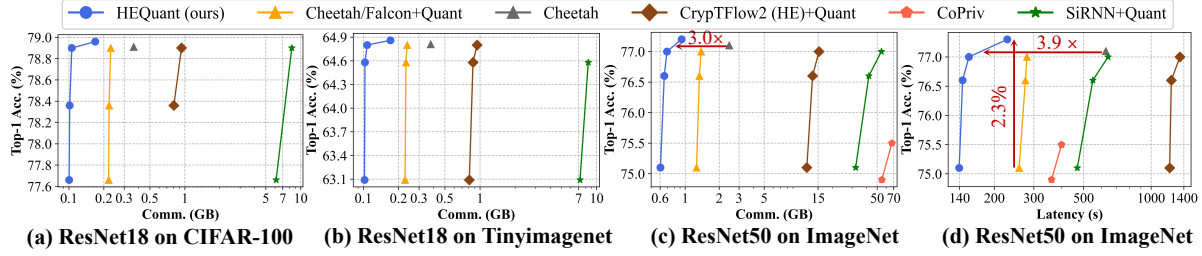


Figure 11. Comparison with prior-art 2PC frameworks on three benchmarks.

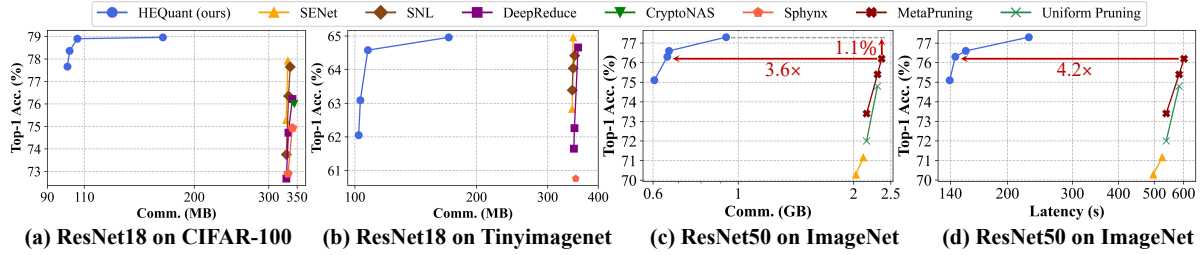


Figure 12. Comparison with prior-art network optimization algorithms on three benchmarks.

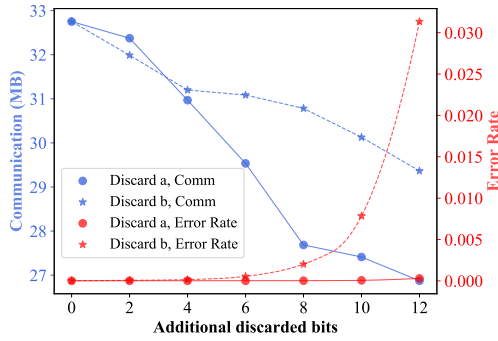


Figure 13. Communication and output error rate for different discarded bits where “Discard a” represents fixing the bit width of b and discarding more bits of a .

trade-off between communication and error rate in output coefficient optimization, we change the number of discarded bits and profile the communication as well as the 1-bit error rate for a convolution from ResNet50. We start with Cheetah and adopt two strategies. The first “Discard a” means we fix the bit width of b and discard more bits of a while “Discard b” means we discard more bits of b . As shown in Figure 13, **1)** the communication cost decreases with the number of discarded bits, while the error rate increases; **2)** the communication cost of “Discard a” is lower than that of “Discard b” with the same additional discarded bits due to larger dimension of a . In addition, we find the error of “Discard a” is lower, and hence, we choose “Discard a” as our strategy and limit the error rate below 0.0005.

Block-wise comparison and ablation for different techniques To understand how different optimizations help improve communication efficiency, we add our proposed op-

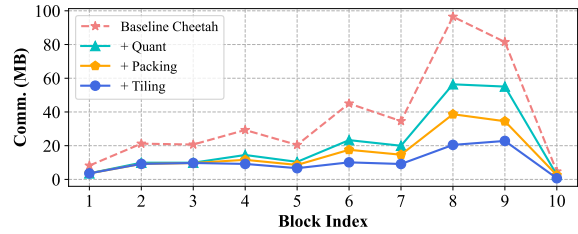


Figure 14. Block-wise visualization of communication on ResNet18 with different optimizations.

timizations step by step and visualize the block-wise communication reduction on ResNet18 and present the results in Figure 14. We can see that **1)** both packing and tiling are effective and help further reduce the communication after quantization; **2)** HEQuant achieves more communication reduction in deeper layers of the network, as H, W becomes smaller and C becomes larger, resulting in a larger tiling optimization space.

6. Conclusion

In this paper, we propose HEQuant, the first 2PC framework that marries low-precision quantization and HE for efficient private inference. HEQuant features an intra-coefficient private packing algorithm and a quantization-aware tiling algorithm to further reduce the communication for low-precision DNNs. Compared with prior-art 2PC frameworks, e.g. Cheetah, HEQuant achieves $3.0\times$ communication and $3.9\times$ latency reduction, respectively. Compared with the prior-art network optimization algorithms, HEQuant can achieve over $3.1\times$ communication reduction with higher accuracy.

HEQuant: Marrying Homomorphic Encryption and Quantization for Communication-Efficient Private Inference

Supplementary Material

A. Network quantization

Quantization is one of the most impactful ways to decrease the computational time and energy consumption of neural networks. In neural network quantization, the weights and activation tensors are stored in lower bit precision than the 16 or 32-bit precision they are usually trained in. When moving from 32 to 8 bits, the memory overhead of storing tensors decreases by a factor of 4 while the computational cost for matrix multiplication reduces quadratically by a factor of 16. Neural networks have been shown to be robust to quantization [13, 40], meaning they can be quantized to lower bit-widths with a relatively small impact on the network’s accuracy. Neural network quantization is an essential step in the model efficiency pipeline for any practical use-case of deep learning [2, 28, 36, 51].

B. Output coefficient optimization

Recall from Section 4.2, a p -bit output m is encrypted into a scalar b and a polynomial a . During decryption, we compute $m = \lfloor (b + \mathbf{a}^T \mathbf{s})P/Q \rfloor$ to reconstruct the output m and we let $m_e = b + \mathbf{a}^T \mathbf{s}$. We observe that discarding the lower bits of b and a before ciphertext transmission can reduce the communication cost and doesn’t affect the correctness of decryption.

Formally, we write the high-end and low-end parts of b and a as $b = b_H 2^{l_b} + b_L$ and $a = a_H 2^{l_a} + a_L$ such that $0 \leq b_L < 2^{l_b}, 0 \leq a_L < 2^{l_a}$. Then $m_e = b_L + \mathbf{a}_L^T \mathbf{s} + b_H 2^{l_b} + \mathbf{a}_H^T \mathbf{s} 2^{l_a}$. And we let $e_L = b_L + \mathbf{a}_L^T \mathbf{s}$. If we discard the low-end parts of b and a , after decryption, we will get $\lfloor (m_e - e_L)P/Q \rfloor = m - \lfloor e_L P/Q \rfloor + \lfloor e P/Q \rfloor$, where $\lfloor e P/Q \rfloor$ will round to 0. Remind that only the upper half of the bits of m are useful, so our goal is to ensure $m \gg \frac{p}{2} \equiv (m - \lfloor e_L P/Q \rfloor) \gg \frac{p}{2}$ where \gg means right shift. We first approximate it by $(m - \lfloor e_L P/Q \rfloor) \gg \frac{p}{2} \approx (m \gg \frac{p}{2}) - (\lfloor e_L P/Q \rfloor \gg \frac{p}{2})$. Therefore, we need to ensure $\lfloor e_L P/Q \rfloor \gg \frac{p}{2} = \lfloor (b_L + \mathbf{a}_L^T \mathbf{s})P/Q \rfloor \gg \frac{p}{2} = 0$. The key here is to find out an upper bound for $\mathbf{a}_L^T \mathbf{s}$. Since the secret vector \mathbf{s} distribute uniformly in $\{0, 1\}^N$ and \mathbf{a}_L distributes uniformly in $[0, 2^{l_a})$. Then the variance of $\mathbf{a}_L^T \mathbf{s}$ is $\text{Var} \approx \frac{2N}{9} (2^{l_a})^2$. Same with Cheetah [18], we use $7\sqrt{\text{Var}}$ as a high-probability upper bound ($\approx 1 - 2^{-38.5}$) on the value $\mathbf{a}_L^T \mathbf{s}$. Finally, the constraint is $(7\sqrt{\frac{2N}{9}} 2^{l_a} + 2^{l_b})P/Q < 2^{\frac{p}{2}}$ and we set $l_b = l' + \frac{p}{2} - 1, l_a = l' + \frac{p}{2} - 1 - \lfloor \log_2(7\sqrt{\frac{2N}{9}}) \rfloor$ to meet the constraint, where $l' = \lfloor \log_2(Q/P) \rfloor$.

However, the approximation of $(m - \lfloor e_L P/Q \rfloor) \gg \frac{p}{2} \approx$

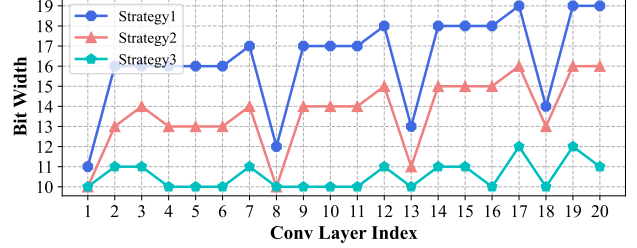


Figure 15. Layer-wise accumulation bit width in ResNet32 with 4-bit for both weight and activation.

$(m \gg \frac{p}{2}) - (\lfloor e_L P/Q \rfloor \gg \frac{p}{2})$ may cause least significant bit (LSB) error. To be more specific, there will be a $1/(2^{q-p/2-\log_2(e_L)})$ probability of causing a 1-bit LSB error. Therefore, we decrease e_L with several tricks to reduce the probability of LSB error. The first trick is to decrease the number of discarded bits of b rather than a because a accounts for larger communication. Moreover, after each linear layer, we need to truncate the output to low bit width b_a where the output will be divided by a scaling factor. That means more low-end bits of the output are useless and can help us reduce the 1-bit error rate. Ultimately, we make the error rate lower than 0.0005 by skipping the low $l' - 1$ of b and the low $l' + \frac{p}{2} - 1 - \sigma$ of a where $\sigma = \lfloor \log_2(7\sqrt{\frac{2N}{9}}) \rfloor$.

C. Visualization of different accumulation bit width reduction strategies

Figure 15 visualizes the layer-wise accumulation bit width in a ResNet18 network trained on the CIFAR-100 dataset with different strategies proposed in Section 4.2.

D. Experiment setting

D.1. Network architecture

We evaluate and compare HEQuant with prior-art methods on three networks on three datasets, and the details of which are shown in Table 6.

D.2. Training details

We train ResNet18 following the training scheme in [2] to use real-valued PyTorch pre-trained models as initialization for corresponding quantized networks. We use Adam optimizer [27] with a cosine learning rate decay scheduler. The initial learning rate is set to $55e - 5$ for weight parameters and batch size is set to 256. We set weight decay to

Table 6. HEQuant evaluation benchmarks.

Model	Layers	# Params (M)	MACs (G)	Dataset
ResNet18	20 Conv, 1 FC, 1 AP, 17 ReLU	11.22	0.558	CIFAR-100/Tinyimagenet
ResNet50	49 CONV, 1 FC, 1, MP, 1 AP, 49 ReLU	2.5	4.1	Imagenet

be $6e - 2$. The models are trained for 400 epochs **without** a knowledge distillation scheme. We adopt the basic data augmentation as ResNet [17]. Training images are randomly resized and cropped to 32×32 pixels (64×64 pixels for Tinyimagenet) and randomly flipped horizontally. Test images are center-cropped to the same resolution.

For ResNet50, we follow [51] with the same training settings. Specifically, with an initial learning rate of 0.1 for the weights and an initial learning rate of 0.01 for the clipping and companding parameters, the models were trained over 120 epochs with a mini-batch size of 512 for ResNet50. In addition, we applied a warm-up method for the first 5 epochs and increased the learning rate linearly from 10^{-4} to the initial value. The weight decay was set to 4×10^{-5} . The training images were resized, cropped to 224×224 pixels and randomly flipped horizontally. The test images were center-cropped to 224×224 pixels.

E. Experimental results of latency

Figure 17 and Figure 18 show the latency comparison with prior-art 2PC frameworks and network optimization algorithms on three benchmarks under LAN and WAN. We can see that: **1)** HEQuant achieves over $3\times$ latency reduction compared with prior-art 2PC frameworks and over $2.5\times$ latency reduction compared with prior-art network optimization algorithms; **2)** Under WAN, HEQuant demonstrates more significant latency reduction than under LAN due to the large communication reduction achieves by HEQuant.

F. Communication comparison on Micro-Benchmark

Same with Section 5.2, we compare the communication cost of HEQuant with CrypTFlow2, Iron, Cheetah, and Falcon for single convolution and depthwise convolution with different dimensions. As shown in Figure 16, HEQuant achieves on average $3.0\times$ communication reduction compared to SOTA Iron. Note that the communication cost of CrypTFlow2 is relatively low. However, CrypTFlow2 uses SIME-based HE and suffers from extremely high latency as shown in Section 5.2.

G. Comparison with Falcon

We compare HEQuant with Falcon on MobileNetV2 in Table 7. Though Falcon is optimized specifically for MobileNetV2, HEQuant still achieves $2.5\times$ communication

Table 7. Comparison with Falcon on MobileNetV2 on the TinyImagenet dataset with W4A4.

MobileNetV2	Comm. (MB)	Latency (s)
Cheetah	561.7 (4.8 \times)	86.3 (3.0 \times)
Falcon	296.9 (2.5 \times)	55.9 (1.9 \times)
HEQuant	118.3	29.0

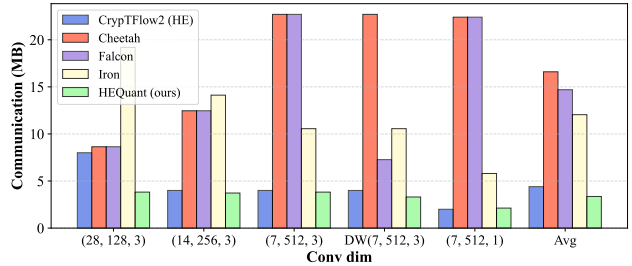


Figure 16. Communication comparison of convolutions of different dimensions (Conv dim represents the input feature height, channels, and kernel size). DW means depthwise convolution and Avg means the average.

and $1.9\times$ latency reduction.

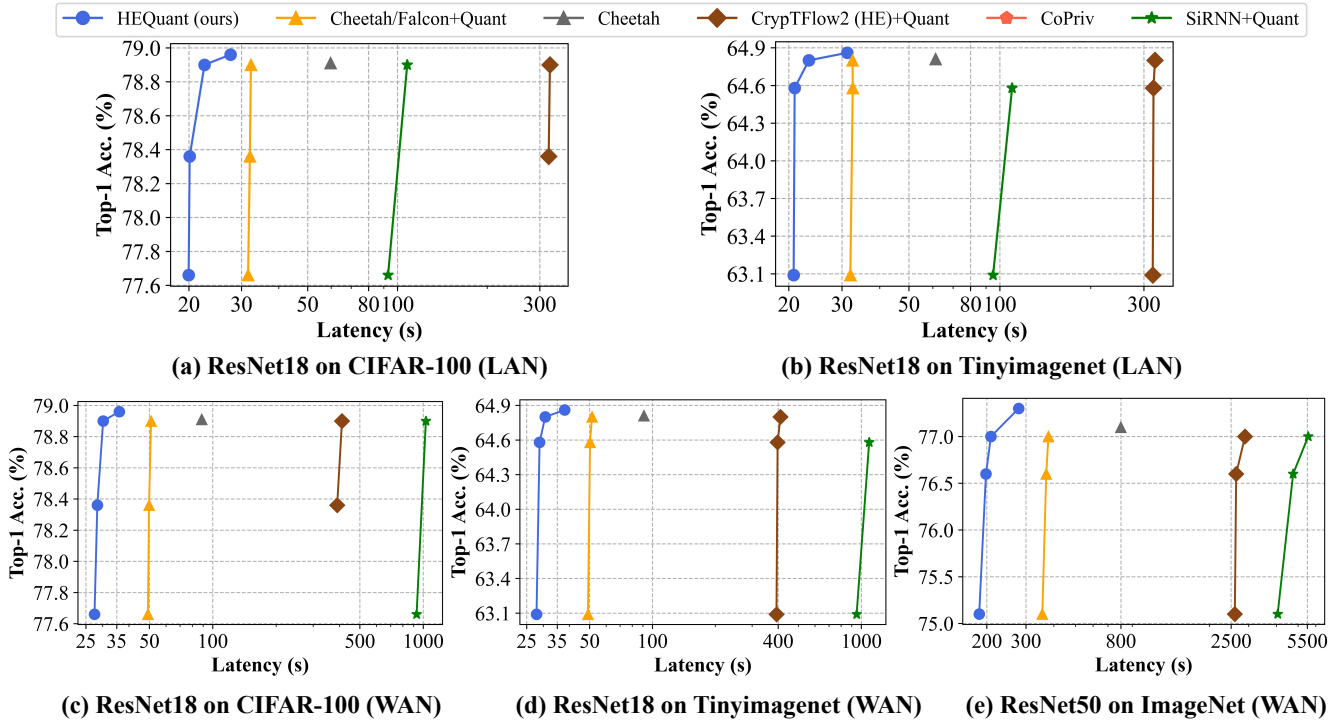


Figure 17. Latency comparison with prior-art 2PC frameworks on three benchmarks under LAN and WAN.

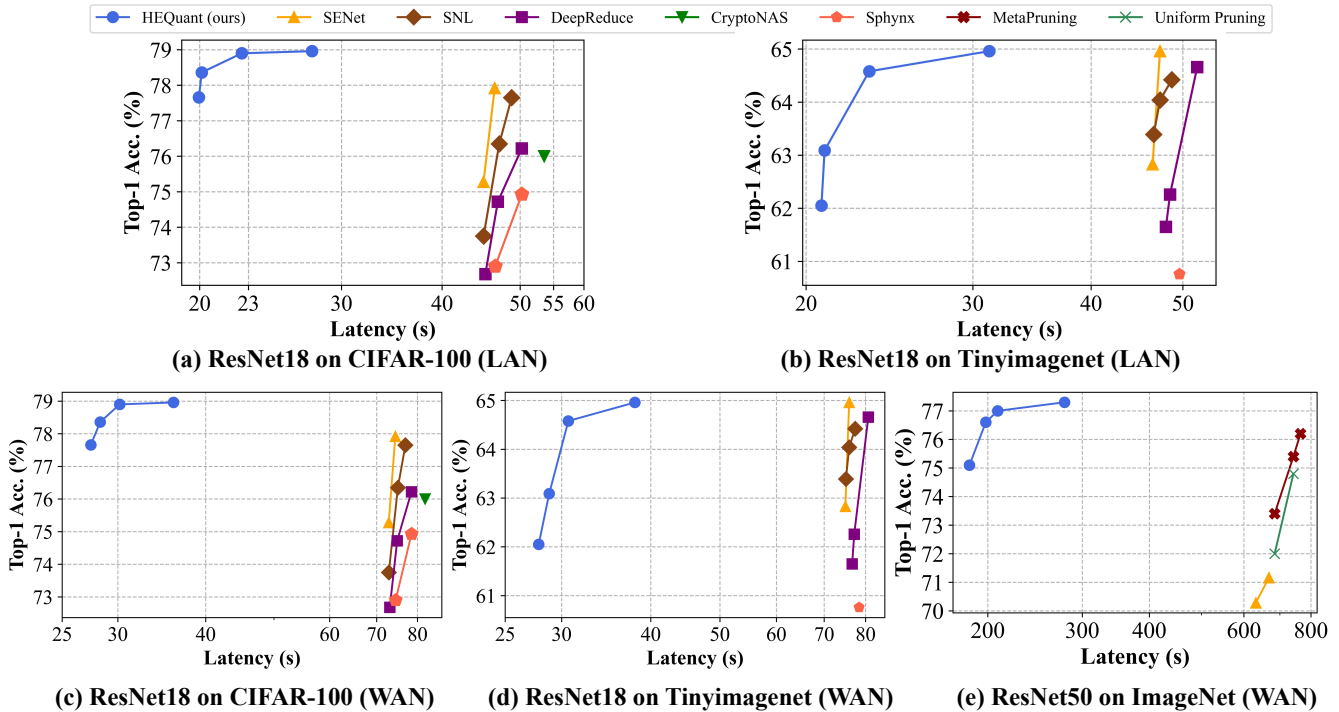


Figure 18. Latency comparison with prior-art network optimization algorithms on three benchmarks under LAN and WAN.

References

- [1] Neda Azouji, Ashkan Sami, and Mohammad Taheri. Efficientmask-net for face authentication in the era of covid-19 pandemic. *Signal, Image and Video Processing*, 16(7): 1991–1999, 2022. [1](#)
- [2] Yash Bhalgat, Jinwon Lee, Markus Nagel, Tijmen Blankevoort, and Nojun Kwak. Lsq+: Improving low-bit quantization through learnable offsets and better initialization. In *Proceedings of the IEEE/CVF Conference on Computer Vision and Pattern Recognition Workshops*, pages 696–697, 2020. [1](#), [6](#), [7](#)
- [3] Thomas M Brill, Laura Munoz, and Richard J Miller. Siri, alexa, and other digital assistants: a study of customer satisfaction with artificial intelligence applications. In *The Role of Smart Technologies in Decision Making*, pages 35–70. Routledge, 2022. [1](#)
- [4] Nishanth Chandran, Divya Gupta, Aseem Rastogi, Rahul Sharma, and Shardul Tripathi. Ezpc: Programmable, efficient, and scalable secure two-party computation for machine learning. *Cryptology ePrint Archive*, 2017. [7](#)
- [5] Minsu Cho, Zahra Ghodsi, Brandon Reagen, Siddharth Garg, and Chinmay Hegde. Sphynx: A deep neural network design for private inference. *IEEE Security & Privacy*, 20(5):22–34, 2022. [2](#)
- [6] Minsu Cho, Ameya Joshi, Brandon Reagen, Siddharth Garg, and Chinmay Hegde. Selective network linearization for efficient private inference. In *International Conference on Machine Learning*, pages 3947–3961. PMLR, 2022. [2](#), [7](#)
- [7] Woo-Seok Choi, Brandon Reagen, Gu-Yeon Wei, and David Brooks. Impala: Low-latency, communication-efficient private deep learning inference, 2022. [1](#)
- [8] Roshan Dathathri, Olli Saarikivi, Hao Chen, Kim Laine, Kristin Lauter, Saeed Maleki, Madanlal Musuvathi, and Todd Mytkowicz. Chet: an optimizing compiler for fully-homomorphic neural-network inferencing. In *Proceedings of the 40th ACM SIGPLAN Conference on Programming Language Design and Implementation*, 2019. [1](#)
- [9] Daniel Demmler, Thomas Schneider, and Michael Zohner. Aby -a framework for efficient mixed-protocol secure two-party computation. In *Proceedings 2015 Network and Distributed System Security Symposium*, 2015. [1](#)
- [10] Zhen Dong, Zhewei Yao, Daiyaan Arfeen, Amir Gholami, Michael W Mahoney, and Kurt Keutzer. Hawq-v2: Hessian aware trace-weighted quantization of neural networks. *Advances in neural information processing systems*, 33:18518–18529, 2020. [1](#)
- [11] Shengyu Fan, Zhiwei Wang, Weizhi Xu, Rui Hou, Dan Meng, and Mingzhe Zhang. Tensorfhe: Achieving practical computation on encrypted data using gpgpu. In *2023 IEEE International Symposium on High-Performance Computer Architecture (HPCA)*, pages 922–934. IEEE, 2023. [2](#)
- [12] Karthik Garimella, Zahra Ghodsi, NandanKumar Jha, Siddharth Garg, and Brandon Reagen. Characterizing and optimizing end-to-end systems for private inference, 2022. [2](#)
- [13] Amir Gholami, Sehoon Kim, Zhen Dong, Zhewei Yao, Michael W Mahoney, and Kurt Keutzer. A survey of quantization methods for efficient neural network inference. In *Low-Power Computer Vision*, pages 291–326. Chapman and Hall/CRC, 2022. [1](#), [4](#)
- [14] Ran Gilad-Bachrach, Nathan Dowlin, Kim Laine, Kristin Lauter, Michael Naehrig, and John Wernsing. Cryptonets: Applying neural networks to encrypted data with high throughput and accuracy. In *International conference on machine learning*, pages 201–210. PMLR, 2016. [1](#), [2](#)
- [15] Kanav Gupta, Deepak Kumaraswamy, Nishanth Chandran, and Divya Gupta. Llama: A low latency math library for secure inference. *Proceedings on Privacy Enhancing Technologies*, 2022(4):274–294, 2022. [1](#)
- [16] Meng Hao, Hongwei Li, Hanxiao Chen, Pengzhi Xing, Guowen Xu, and Tianwei Zhang. Iron: Private inference on transformers. In *Advances in Neural Information Processing Systems*, 2022. [1](#), [2](#), [3](#), [4](#), [7](#)
- [17] Kaiming He, Xiangyu Zhang, Shaoqing Ren, and Jian Sun. Deep residual learning for image recognition. In *2016 IEEE Conference on Computer Vision and Pattern Recognition (CVPR)*, 2016. [2](#)
- [18] Zhicong Huang, Wen-jie Lu, Cheng Hong, and Jiansheng Ding. Cheetah: Lean and fast secure {Two-Party} deep neural network inference. In *31st USENIX Security Symposium (USENIX Security 22)*, pages 809–826, 2022. [1](#), [2](#), [3](#), [4](#), [6](#), [7](#)
- [19] Siam Umar Hussain, Mojan Javaheripi, Mohammad Samragh, and Farinaz Koushanfar. Coinn: Crypto/ml codesign for oblivious inference via neural networks. In *Proceedings of the 2021 ACM SIGSAC Conference on Computer and Communications Security*, pages 3266–3281, 2021. [2](#)
- [20] Nandan Kumar Jha, Zahra Ghodsi, Siddharth Garg, and Brandon Reagen. Deepreduce: Relu reduction for fast private inference. In *International Conference on Machine Learning*, pages 4839–4849. PMLR, 2021. [2](#), [7](#)
- [21] Chiraag Juvekar, Vinod Vaikuntanathan, and AnanthaP. Chandrakasan. GAZELLE: A low latency framework for secure neural network inference, 2018. [1](#), [2](#)
- [22] Georgios Kaissis, Alexander Ziller, Jonathan Passerat-Palmbach, Théo Ryffel, Dmitrii Usynin, Andrew Trask, Ionésio Lima Jr, Jason Mancuso, Friederike Jungmann, Marc-Matthias Steinborn, et al. End-to-end privacy preserving deep learning on multi-institutional medical imaging. *Nature Machine Intelligence*, 3(6):473–484, 2021. [1](#)
- [23] Dongwoo Kim and Cyril Guyot. Optimized privacy-preserving cnn inference with fully homomorphic encryption. *IEEE Transactions on Information Forensics and Security*, 18:2175–2187, 2023. [2](#)
- [24] Donghwan Kim, Jaiyoung Park, Jongmin Kim, Sangpyo Kim, and JungHo Ahn. Hypen: A hybrid packing method and optimizations for homomorphic encryption-based neural networks, 2023. [1](#)
- [25] Donghwan Kim, Jaiyoung Park, Jongmin Kim, Sangpyo Kim, and Jung Ho Ahn. Hypen: A hybrid packing method and optimizations for homomorphic encryption-based neural networks. *arXiv preprint arXiv:2302.02407*, 2023. [2](#)
- [26] Jongmin Kim, Gwangho Lee, Sangpyo Kim, Gina Sohn, Minsoo Rhu, John Kim, and Jung Ho Ahn. Ark: Fully homomorphic encryption accelerator with runtime data generation and inter-operation key reuse. In *2022 55th IEEE/ACM Inter-*

- national Symposium on Microarchitecture (MICRO)*, pages 1237–1254. IEEE, 2022. **2**
- [27] DiederikP. Kingma and Jimmy Ba. Adam: A method for stochastic optimization. *arXiv: Learning, arXiv: Learning*, 2014. **1**
- [28] Raghuraman Krishnamoorthi. Quantizing deep convolutional networks for efficient inference: A whitepaper. *arXiv preprint arXiv:1806.08342*, 2018. **4, 1**
- [29] Nishant Kumar, Mayank Rathee, Nishanth Chandran, Divya Gupta, Aseem Rastogi, and Rahul Sharma. Cryptflow: Secure tensorflow inference. In *2020 IEEE Symposium on Security and Privacy (SP)*, pages 336–353. IEEE, 2020. **1**
- [30] Souvik Kundu, Shunlin Lu, Yuke Zhang, Jacqueline Liu, and Peter A Beerel. Learning to linearize deep neural networks for secure and efficient private inference. *arXiv preprint arXiv:2301.09254*, 2023. **2, 7**
- [31] Eunsang Lee, Joon-Woo Lee, Junghyun Lee, Young-Sik Kim, Yongjune Kim, Jong-Seon No, and Woosuk Choi. Low-complexity deep convolutional neural networks on fully homomorphic encryption using multiplexed parallel convolutions. In *International Conference on Machine Learning*, pages 12403–12422. PMLR, 2022. **2**
- [32] Joon-Woo Lee, HyungChul Kang, Yongwoo Lee, Woosuk Choi, Jieun Eom, Maxim Deryabin, Eunsang Lee, Junghyun Lee, Donghoon Yoo, Young-Sik Kim, et al. Privacy-preserving machine learning with fully homomorphic encryption for deep neural network. *IEEE Access*, 10:30039–30054, 2022. **2**
- [33] Ryan Lehmkuhl, Pratyush Mishra, Akshayaram Srinivasan, and Raluca Ada Popa. Muse: Secure inference resilient to malicious clients. In *30th USENIX Security Symposium (USENIX Security 21)*, pages 2201–2218, 2021. **2**
- [34] Jian Liu, Mika Juuti, Yao Lu, and N. Asokan. Oblivious neural network predictions via minion transformations. In *Proceedings of the 2017 ACM SIGSAC Conference on Computer and Communications Security*, 2017. **2**
- [35] Zechun Liu, Haoyuan Mu, Xiangyu Zhang, Zichao Guo, Xin Yang, Kwang-Ting Cheng, and Jian Sun. Metapruning: Meta learning for automatic neural network channel pruning. In *Proceedings of the IEEE/CVF international conference on computer vision*, pages 3296–3305, 2019. **2, 7**
- [36] Zechun Liu, Kwang-Ting Cheng, Dong Huang, Eric P Xing, and Zhiqiang Shen. Nonuniform-to-uniform quantization: Towards accurate quantization via generalized straight-through estimation. In *Proceedings of the IEEE/CVF Conference on Computer Vision and Pattern Recognition*, pages 4942–4952, 2022. **1, 4, 6**
- [37] Wen-jie Lu, Zhicong Huang, Zhen Gu, Jingyu Li, Jian Liu, Kui Ren, Cheng Hong, Tao Wei, and WenGuang Chen. Bumblebee: Secure two-party inference framework for large transformers. *Cryptology ePrint Archive*, 2023. **2, 3**
- [38] Pratyush Mishra, Ryan Lehmkuhl, Akshayaram Srinivasan, Wenting Zheng, and RalucaAda Popa. Delphi: A cryptographic inference service for neural networks, 2020. **2, 3**
- [39] Payman Mohassel and Yupeng Zhang. Secureml: A system for scalable privacy-preserving machine learning. In *2017 IEEE symposium on security and privacy (SP)*, pages 19–38. IEEE, 2017. **2, 7**
- [40] Markus Nagel, Marios Fournarakis, Rana Ali Amjad, Yelysei Bondarenko, Mart Van Baalen, and Tijmen Blankevoort. A white paper on neural network quantization. *arXiv preprint arXiv:2106.08295*, 2021. **4, 1**
- [41] George Onoufriou, Paul Mayfield, and Georgios Leontidis. Fully homomorphically encrypted deep learning as a service. *Machine Learning and Knowledge Extraction*, 3(4): 819–834, 2021. **2**
- [42] Jaiyoung Park, Donghwan Kim, Jongmin Kim, Sangpyo Kim, Wonkyung Jung, Jung Hee Cheon, and Jung Ho Ahn. Toward practical privacy-preserving convolutional neural networks exploiting fully homomorphic encryption. *arXiv preprint arXiv:2310.16530*, 2023. **2**
- [43] Haotong Qin, Ruihao Gong, Xianglong Liu, Xiao Bai, Jingkuan Song, and Nicu Sebe. Binary neural networks: A survey. *Pattern Recognition*, 105:107281, 2020. **4**
- [44] Haotong Qin, Ruihao Gong, Xianglong Liu, Mingzhu Shen, Ziran Wei, Fengwei Yu, and Jingkuan Song. Forward and backward information retention for accurate binary neural networks. In *Proceedings of the IEEE/CVF conference on computer vision and pattern recognition*, pages 2250–2259, 2020. **4**
- [45] Deevashwer Rathee, Mayank Rathee, Nishant Kumar, Nishanth Chandran, Divya Gupta, Aseem Rastogi, and Rahul Sharma. Cryptflow2: Practical 2-party secure inference. In *Proceedings of the 2020 ACM SIGSAC Conference on Computer and Communications Security*, pages 325–342, 2020. **2, 3, 7**
- [46] Deevashwer Rathee, Mayank Rathee, Rahul Kranti Kiran Goli, Divya Gupta, Rahul Sharma, Nishanth Chandran, and Aseem Rastogi. Sirnn: A math library for secure rnn inference. In *2021 IEEE Symposium on Security and Privacy (SP)*, pages 1003–1020. IEEE, 2021. **2, 3, 4, 6, 7**
- [47] SEAL. Microsoft SEAL (release 3.6). <https://github.com/Microsoft/SEAL>, 2020. Microsoft Research, Redmond, WA. **6**
- [48] Liyan Shen, Ye Dong, Binxing Fang, Jinqiao Shi, Xuebin Wang, Shengli Pan, and Ruisheng Shi. Abnn 2. In *Proceedings of the 59th ACM/IEEE Design Automation Conference*, 2022. **7**
- [49] Xiao Wang, Alex J. Malozemoff, and Jonathan Katz. EMP-toolkit: Efficient MultiParty computation toolkit. <https://github.com/emp-toolkit>, 2016. **6**
- [50] Tianshi Xu, Meng Li, Runsheng Wang, and Ru Huang. Falcon: Accelerating homomorphically encrypted convolutions for efficient private mobile network inference. *arXiv preprint arXiv:2308.13189*, 2023. **1, 2, 3, 4, 7**
- [51] Kohei Yamamoto. Learnable companding quantization for accurate low-bit neural networks. In *Proceedings of the IEEE/CVF conference on computer vision and pattern recognition*, pages 5029–5038, 2021. **1, 6, 7, 2**
- [52] Zhewei Yao, Zhen Dong, Zhangcheng Zheng, Amir Gholami, Jiali Yu, Eric Tan, Leyuan Wang, Qijing Huang, Yida Wang, Michael Mahoney, et al. Hawq-v3: Dyadic neural network quantization. In *International Conference on Machine Learning*, pages 11875–11886. PMLR, 2021. **1**

- [53] Chunyu Yuan and Sos S Aghaian. A comprehensive review of binary neural network. *Artificial Intelligence Review*, pages 1–65, 2023. [4](#)
- [54] Wenxuan Zeng, Meng Li, Haichuan Yang, Wen-jie Lu, Runsheng Wang, and Ru Huang. Copriv: Network/protocol co-optimization for communication-efficient private inference. *arXiv preprint arXiv:2311.01737*, 2023. [7](#)